





Greigite (Fe₃S₄) is thermodynamically stable: Implications for its terrestrial and planetary occurrence

Tamilarasan Subramani^{a,1}, Kristina Lilova^{a,1}, Mykola Abramchuk^a, Kurt D. Leinenweber^a , and Alexandra Navrotsky^{a,2} 

^aSchool of Molecular Sciences and Center for Materials of the Universe, Arizona State University, Tempe, AZ 85281

Contributed by Alexandra Navrotsky, September 29, 2020 (sent for review August 18, 2020; reviewed by Robert M. Hazen and Juraj Majzlan)

Iron sulfide minerals are widespread on Earth and likely in planetary bodies in and beyond our solar system. Using measured enthalpies of formation for three magnetic iron sulfide phases: bulk and nanophase Fe₃S₄ spinel (greigite), and its high-pressure monoclinic phase, we show that greigite is a stable phase in the Fe–S phase diagram at ambient temperature. The thermodynamic stability and low surface energy of greigite supports the common occurrence of fine-grained Fe₃S₄ in many anoxic terrestrial settings. The high-pressure monoclinic phase, thermodynamically metastable below about 3 GPa, shows a calculated negative P–T slope for its formation from the spinel. The stability of these three phases suggests their potential existence on Mercury and their magnetism may contribute to its present magnetic field.

greigite | thermodynamic stability | terrestrial planets | magnetism | high pressure

Iron sulfides are widespread in the Earth and may be important on other planets. The spinel mineral greigite Fe₃S₄, the sulfide analogs of magnetite Fe₃O₄, has long been considered a metastable phase and a rare mineral (1). Nevertheless, fine-grained Fe₃S₄ has been reported in a variety of geologic and environmental settings. Greigite, mackinawite FeS_{0.9}, and pyrite FeS₂ can be found in sediments formed as a product of sulfate reduction (2). Fine-grained magnetic iron sulfides such as greigite and pyrrhotite have been reported in marine sediments associated with anaerobic oxidation of methane and formation of methane hydrates (3). Small greigite particles occur in magnetotactic bacteria, which produce both Fe₃S₄ and Fe₃O₄ in magnetosome organelles (4). Greigite is a possible catalyst for CO₂ reduction of small organic molecules and for H₂ and CO₂ fixation, relevant to the origin of life (5, 6). Fe₃S₄ can possibly host remanent magnetism, thus potentially contributing to the weak magnetic field of the planet Mercury (7). Greigite has been reported to form as one of the products in the corrosion of crude oil tanks when the rust reacts with H₂S gas above the crude oil surface (8). Given this widespread occurrence, one must question the assumptions of rarity and metastability.

The change of mineral properties with particle size has been recognized as a critical aspect of geochemical and biochemical reactions in natural systems (9). An important question is whether greigite, a sulfide spinel, has a relatively low surface energy analogous to that of magnetite and other oxide spinels (10, 11). If the surface energy of greigite is lower than that of other sulfides in the Fe–S system, its stability at the nanoscale may be enhanced. Particle-size decrease also results in shift to lower oxygen fugacity of the Fe–Si–O oxygen buffers (11). The sulfur and oxygen fugacities are directly linked and control the partitioning of metals between sulfide and oxide phases. Hence, the f_{S2} and f_{S2}–f_{O2} buffers could be affected by particle-size effects in the iron sulfides, oxides, and silicates (12).

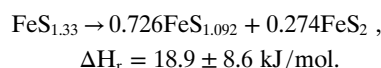
Greigite transforms from a cubic spinel structure to a monoclinic Cr₃S₄-type structure at 3–4 GPa (13, 14). A natural nanosized monoclinic Fe₃S₄ phase, probably the same as the reported high-pressure phase, has been found in the Sudbury ore deposit (15).

Up to now the thermodynamic properties of greigite have not been determined experimentally. Using high-temperature oxide melt solution calorimetric techniques developed for sulfides

(16–19), we determined the energetic stability of bulk, nano-sized, and high-pressure Fe₃S₄ phases. We conclude that greigite is a thermodynamically stable phase in the Fe–S system near ambient temperature, that it has a low surface energy comparable to that of magnetite and other oxide spinels, and that the monoclinic phase has a field of thermodynamic stability above about 3 GPa. Implications for the occurrence of Fe₃S₄ in terrestrial and planetary settings are discussed.

Results and Discussion

All thermodynamic data in this paper are calculated on the basis of 1 mole of iron to facilitate comparison between different iron sulfides. Using the obtained calorimetric data (Table 1), we calculated the enthalpy of decomposition of greigite to the neighboring phases (pyrite and pyrrhotite) without the involvement of either sulfur or iron as separate phases. The free energy of this potential disproportionation reaction holds the key to whether greigite is stable or metastable on the iron–sulfur phase diagram.



The reaction is energetically substantially unfavorable and would require a positive entropy change of >63.4 J/mol.K at 300 K to

Significance

The new experimental thermodynamic studies of bulk, nanophase, and monoclinic high-pressure forms of greigite (Fe₃S₄) confirm its stability in the Fe–S system and explain its common occurrence in sediments, magnetotactic bacteria, and other ambient temperature environments under anoxic conditions. The data disprove the commonly held hypothesis that greigite is a metastable phase. The low surface energy of greigite provides insight not only into the stability of greigite nanoparticles but also into their role in prebiotic, biological, and planetary processes. Our experimental data for the stability of the three forms of Fe₃S₄ confirm that it could be stable on Mercury, thus contributing to Mercury's weak magnetic field.

Author contributions: K.L. and A.N. designed research; T.S., K.L., M.A., K.D.L., and A.N. performed research; T.S., K.L., M.A., K.D.L., and A.N. analyzed data; T.S., K.L., M.A., K.D.L., and A.N. wrote the paper; T.S., M.A., and K.D.L. carried out the synthesis, characterization, and surface area measurements of various Fe₃S₄ phases, did calorimetric measurements, and carried out the synthesis, characterization, and surface area measurements of various Fe₃S₄ phases.

Reviewers: R.M.H., Carnegie Institution for Science; and J.M., Mineralogy Department, University of Jena.

The authors declare no competing interest.

Published under the PNAS license.

¹T.S. and K.L. contributed equally to this work.

²To whom correspondence may be addressed. Email: Alexandra.Navrotsky@asu.edu.

This article contains supporting information online at <https://www.pnas.org/lookup/suppl/doi:10.1073/pnas.2017312117/-DCSupplemental>.

First published November 2, 2020.

Table 1. Enthalpies of drop solution and of formation from elements of iron sulfide phases per mole of iron

Compound	ΔH_{ds} (kJ/mol)	$\Delta H_{f,el}$ (kJ/mol)	Reference
FeS ₂ (pyrite)	$-1,471.1 \pm 4.2$	-175.5 ± 6.0	Xu and Navrotsky, 2010 (16)
FeS (troilite)	-913.5 ± 3.3	-101.4 ± 4.0	Xu and Navrotsky, 2010 (16)
FeS _{1.092} (pyrrhotite)	-966.3 ± 3.3	-106.2 ± 3.5	Xu and Navrotsky, 2010 (16)
FeS _{1.33} (1/3 Fe ₃ S ₄)*			
Bulk (greigite)	$-1,071.6 \pm 6.2$ (6) [†]	-144.1 ± 7.3 [‡]	This work
Nanophase (greigite)	$-1,074.5 \pm 4.3$ (7)	-141.2 ± 5.9	This work
High pressure (monoclinic)	$-1,085.7 \pm 5.6$ (8)	-130.0 ± 6.9	This work

*The data reported refer to the molecular formula FeS_{1.33}.

[†]Number of drops given in parentheses; error is 2 SDs of the mean.

[‡]The thermochemical cycle used to calculate the enthalpies of formation is given in *SI Appendix, Table S2*.

change the sign of ΔG . Although the standard entropy of greigite is not known, such a large ΔS is very unlikely for a reaction involving only solid phases. We conclude that greigite is a stable phase in the iron–sulfur system, at least near ambient temperature, and it warrants a place on the equilibrium iron–sulfur phase diagram. Greigite is known as an intermediate in pyrite formation, (pyritization) under anoxic sulfate-reducing sedimentary conditions (1, 20). Under a diluted carbon supply, the iron species will react with sulfide produced by anaerobic decomposition of organic matter until the reactive iron exhausts the available sulfide and stops the reaction, thus resulting in preservation of greigite (21). The formation of pyrite from greigite will occur, not because greigite is intrinsically metastable at its own composition, but because excess sulfur is present. Our thermodynamic data support the idea (21) that greigite is a stable compound once formed unless there is a change in sulfidizing environment, which explains its common occurrence in a number of terrestrial environments (ref. 1 and references therein). Since greigite is also frequently preserved in the geologic record, it can be a potential indicator of the paleo-chemistry of lakes or marine environments (22).

In order to further constrain greigite stability, the effect of the particle-size decrease on the energetics must be considered. Natural greigite, particularly that formed in sediments (3) and from bacteria (4) is predominantly fine grained, i.e., nanosized, with typical particle size of 30–70 nm. We measured the surface energy of greigite from the difference in enthalpy of drop solution of bulk and nanophase samples, as described in *SI Appendix*, to be 1.15 J/m² (estimated error of surface energy is 20%, refer to *SI Appendix*), similar to values for magnetite and other oxide spinels, which range between 0.80 and 1.20 J/m² (10, 23, 24), and are generally smaller than values for other possible competing oxide phases.

Both magnetite and greigite are produced as small particles by magnetotactic bacteria and their relatively small surface energies suggest relatively little driving force for coarsening (4). Moreover, some magnetotactic bacteria produce only nanocrystalline greigite (between 30 and 70 nm diameter), which does not convert to pyrite even in the presence of excess H₂S (25). Thus, it is possible that the small surface energy of the sulfide spinel extends its stability field relative to pyrite in the Fe–S system, analogous to effects seen with magnetite in the Fe–O and Fe–O–SiO₂ systems (10, 11). To quantify this possible effect, and analogous effects on the pyrrhotite–greigite equilibrium, one would need to know the surface energy of pyrite and pyrrhotite. Experimental measurements of these values do not yet exist. There have been two calculations of the surface energy of pyrite (26, 27), but none for pyrrhotite. They use density-functional theory and molecular mechanics methods, and they show considerable scatter, rely on differing assumptions, and are not directly comparable to experimental values. Thus, although qualitatively it appears likely that the low surface energy of Fe₃S₄ spinel aids in stabilizing it thermodynamically at the nanoscale, quantitation is not yet possible.

The surface energetics of greigite might be important for the catalytic formation of prebiotic organic molecules on its surface and thus for the origin of life according to the iron–sulfur world hypothesis (6). The cubic Fe₄S₄ units resemble 4Fe–4S clusters, which are found in the proteins of all living organisms and act as catalysts for synthesis of biomolecules (28).

The low oxygen fugacity and the high sulfur concentration recorded during the MESSENGER mission support possible widespread presence of iron sulfide phases on Mercury (29, 30) due to the lack of atmosphere, slow rotation, and high eccentricity, the surface temperature of Mercury varies considerably. While the highest temperature on the surface at the equator could reach 700 K, the temperature at depths below 1 m is modeled to be 450 K or less (31), while the temperature in polar craters could drop to 100 K. Thus, the surface and near-surface regions of Mercury are likely to be within the stability field of greigite.

Greigite shows stable magnetic properties with no phase transitions at low temperature (32). Greigite may not be the only iron sulfide existing on Mercury, but it is one of the compounds with sufficiently high Curie temperature (610 K) to remain magnetic in the upper crust and host the remanent magnetization (7). Pyrite is weakly paramagnetic with a small and positive susceptibility (33), thus it would not be relevant to the crustal magnetization. Troilite is antiferromagnetic and not expected to hold magnetic remanence (34). Pyrrhotite has a Curie temperature of about 600 K (35) so it, as well as greigite, could contribute to magnetic remanence.

The relevance of greigite nanoparticles to Mercury stems from the estimated abundance of nanoparticles on Mercury, which is a potential explanation for its dark surface and relatively featureless visible and near-infrared spectra (36). Constant surface bombardment by bolides and the solar wind (36, 37) could further enhance greigite nanoparticle formation. The low surface energy would provide little driving force for grain growth. Nanoparticulate Fe₃S₄ therefore becomes a highly possible magnetic mineral present on the surface of Mercury with single or pseudosingle domains holding the remanent magnetism from the planet's ancient magnetic field (1, 35, 38).

Although chondritic meteorites are commonly considered as building blocks for terrestrial planets, it is unlikely that a large planet will retain the same exact chemistry as its building blocks with the change in oxygen fugacity, temperature, and pressure (39). The phase equilibria of the compounds in the Fe–S system will dramatically shift with changes in the oxygen and sulfur fugacities. Thus, although greigite is not commonly found in meteorites, that is not a definitive argument against its existence on Mercury, especially bearing in mind the reported high sulfur content there. Indeed, greigite has been found in meteorites previously, usually as a fine-grained material, coexisting with other iron phases such as pyrrhotite and magnetite. McKay et al. (40) suggested the presence of nanogreigite with postulated biogenic origin in a Martian meteorite. They could not obtain conclusive transmission electron

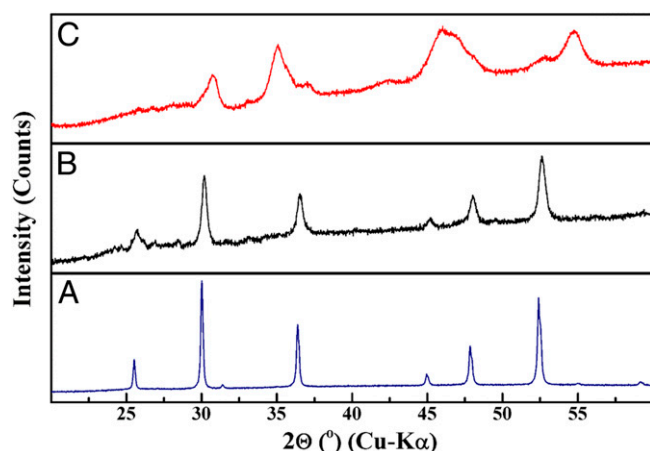


Fig. 1. PXRD patterns of three Fe_3S_4 phases: bulk (A) and nano- (B) greigite with spinel ($Fd\text{-}3m$) structure. The bulk greigite (A) was compressed under a pressure of 5 GPa in multianvil press to obtain high-pressure monoclinic phase ($I2/m$). PXRD pattern of high-pressure monoclinic phase is given in C. The observed high background in the diffraction pattern originates from Fe fluorescence.

microscopy (TEM) results, because the particles were unstable in the electron beam. Greigite was also found in the stony meteorite El Hammami, stony-Fe meteorite Gujba, and Fe meteorite from Canyon Diablo, where it was mixed with seven other minerals (41). The difficulties in characterizing fine-grained greigite in meteorites suggest that it might have more common occurrence than has been assumed, but has been overlooked or not properly identified.

We have confirmed the existence of the high-pressure monoclinic Fe_3S_4 phase (13–15), which is supposed to be ferrimagnetic like the cubic spinel (13, 15). We synthesized the material at 5 GPa and ambient temperature in a multianvil press to investigate its structure and thermodynamics (Fig. 1). The enthalpy of transition from greigite to the high-pressure phase, measured by oxide melt solution calorimetry, is endothermic: 14.1 ± 8.3 kJ/mol per $\text{Fe}_{1.33}$ formula unit, and the change in molar volume is -10.46 ± 0.22 $\text{cm}^3\text{mol}^{-1}$. According to Susilo et al. (14), the high-pressure monoclinic phase starts appearing above 3 GPa at ambient temperature and the cubic phase is completely transformed to the monoclinic phase at 6 GPa. The transition has not been reversed. Assuming that the spread over a range of pressures reflects slow transformation kinetics, we take the onset of the transition at 3 GPa as a “half bracket,” meaning that the equilibrium transition pressure is at or below 3 GPa. Then, the free energy of transition at 3 GPa would be zero, and $\Delta G(3 \text{ GPa}) = 0 = \Delta H - T\Delta S + P\Delta V$, to a first approximation. This gives $\Delta S = 12.2 \pm 2.8$ J/mol. K. Thus the high-pressure phase has a lower volume but a higher entropy than greigite, giving, according to the Clausius–Clapeyron equation $(dP/dT)_{\text{equil}} = \Delta S/\Delta V = -0.0035 \pm 0.0008$ GPa/K. This negative P-T slope (Fig. 2) would suggest higher pressure for the transition in colder regions of a planet like Mercury but lower pressures in warmer regions. If the true transition pressure is lower than 3 GPa, the entropy change would become even more positive.

Monoclinic Fe_3S_4 was predicted to undergo a half-metal to metallic transition upon compression (13), but electrical transport measurements showed only semiconducting behavior in the high-pressure phase (14). The experimental studies have indeed shown a drop in resistivity to 4–6 m Ωcm upon compression above 2 GPa. Although relatively low, this resistivity is higher than for a typical metal. This complex resistivity behavior is attributed to the enhancement of electron hopping between Fe^{2+} and Fe^{3+} ions mediated by polarons (14). The mobility of polarons is increased by compression. The electron hopping and polaron mobility represent delocalization of electrons and could result in a higher

entropy of the high-pressure phase and account for the negative P-T slope of the transition.

Although the high-pressure transition has not been reversed, the positive enthalpy of transition shows that cubic greigite spinel is clearly stable at atmospheric pressure and 298 K. The monoclinic and cubic phases would coexist stably only at the phase-boundary pressures and temperatures. This is consistent with the natural monoclinic phase in the Sudbury ore deposit being accompanied by pyrrhotite (Fe_{1-x}S), but not by cubic Fe_3S_4 (15). The presence of the monoclinic phase in the Sudbury, Ontario, Canada impact structure is consistent with it being a quench product from high pressures, higher than the equilibrium phase boundary. Interestingly, both that material and our synthetic sample appear to have very small crystallite size and nanoscale phenomena may contribute to their formation and energetics. Another possible implication could be a potential existence of monoclinic Fe_3S_4 in the lower crust or at the crust–mantle boundary of Mercury.

In summary, our experimental thermodynamic results illustrate the complex nature of phase behavior in the Fe–S system. We conclude that Fe_3S_4 spinel (greigite) is a stable phase near ambient conditions in the Fe–S system, that it has a low surface energy comparable to that of oxide spinels, and that it transforms, with a negative P-T slope to a high-pressure monoclinic phase near 3 GPa. These results suggest that Fe_3S_4 is not a rare metastable mineral but may occur commonly as a stable phase, often as nanoparticles, in a number of terrestrial and planetary environments.

Materials and Methods

Materials. Iron (II) chloride tetrahydrate (Alfa Aesar), L-cysteine (Fisher Scientific), hexadecyltrimethylammonium bromide (CTAB) (Fisher Scientific), polyvinylpyrrolidone (PVP) (Alfa Aesar), ethylenediamine (Fisher Scientific), and deionized water which was purged with nitrogen gas for 1 h.

Synthesis. Bulk Fe_3S_4 was synthesized by hydrothermal method following previously reported procedure (42). Inside a glove tent, 8 mmol of iron (II) chloride tetrahydrate, 12 mmol of L-cysteine, and 2.4 mmol of CTAB were dissolved in 140 mL of N_2 -purged deionized water. The mixture is then transferred to a 200-mL Teflon container and sealed inside an autoclave. The autoclave was heated to 165 °C for 40 h and cooled naturally. A black precipitate was obtained by centrifugation and washed with water and ethanol several times. The precipitate was finally dried at room temperature.

For nano- Fe_3S_4 synthesis, a previously reported procedure with a slight modification was carried out (43–45). In a 250-mL three-neck flask, 16 mmol of L-cysteine and 2 mmol of PVP were dissolved in 70 mL of deionized water under degassing with nitrogen. Eight mmol of iron (II) chloride tetrahydrate was dissolved in 70 mL of deionized water in separate beaker and added to the three-neck flask drop by drop using a syringe. Finally, 500 μL of ethylene

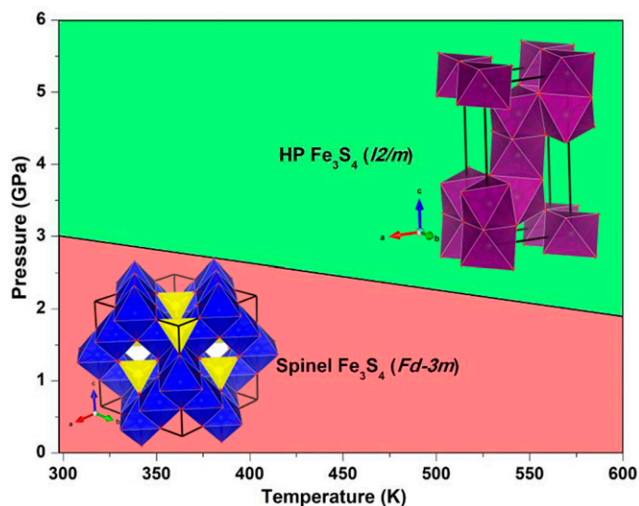


Fig. 2. Calculated P-T diagram of Fe_3S_4 showing negative slope.

diamine was added to the mixture and stirred well. The resulting mixture was transferred to a 200-mL Teflon sealed autoclave and heated at 160 °C for 16 h. The resulting black precipitate was washed with water and ethanol several times before being allowed to dry at room temperature.

Two preparations were done in a multianvil press (Big Blue Press at Arizona State University) to produce enough of the high-pressure phase for calorimetric and other measurements. The samples were run in an 18/12 multianvil assembly at room temperature and 5 GPa (46). The samples were compressed to 5 GPa, held at pressure overnight, and then decompressed, all at room temperature, and the product consisted of the high-pressure phase of Fe₃S₄. The samples were recovered as well-compacted and coherent pellets. Boron nitride capsules were used to contain the samples, and the boron nitride layers were easily separated from the sample pellets after the syntheses. The total yield was about 300 mg of high-pressure Fe₃S₄.

Characterization. The phase purity of Fe₃S₄ samples was checked by powder X-ray diffraction (PXRD) with a Bruker D8 Advance diffractometer with Cu K α radiation (40 kV, 40 mA) in the 2 θ range of 10–80° with a 0.018° step size and a 1-s step time. The PXRD patterns were refined by employing the

program GSAS-II (47), and Jade software (version 6.11, 2002; Materials Data Inc.) to check the phase purity and the crystallite size. VESTA software was employed to generate crystal structures using the data obtained from Rietveld refinement (48). Specific surface area measurements were done by N₂ adsorption at –196 °C using the five-point Brunauer–Emmett–Teller technique in Micromeritics Gemini VII 2390 surface area analyzer to obtain the particle size. Before the analysis, 60 mg of sample was made into pellets and degassed at 150 °C for 16 h.

High-Temperature Oxide Melt Solution Calorimetry. High-temperature oxide melt solution calorimetry was performed using a Tian-Calvet twin calorimeter AlexSYS at 800 °C. The procedure has been described in detail before (18, 49–51).

Data Availability. All study data are included in the article and [SI Appendix](#).

ACKNOWLEDGMENTS. This study was supported by the US Department of Energy, Office of Science, Office of Basic Energy Sciences, Chemical Sciences, Geosciences, and Biosciences Division under Award DE-FG02-97ER14749.

1. A. P. Roberts, L. Chang, C. J. Rowan, C.-S. Horng, F. Florindo, Magnetic properties of sedimentary greigite (Fe₃S₄): An update. *Rev. Geophys.* **49**, RG1002 (2011).
2. J. Liu *et al.*, Formation and preservation of greigite (Fe₃S₄) in a thick sediment layer from the central south Yellow Sea. *Geophys. J. Int.* **213**, 135–146 (2018).
3. M. Rudmin *et al.*, Ferrimagnetic iron sulfide formation and methane venting across the Paleocene-Eocene thermal maximum in shallow marine sediments, ancient west Siberian sea. *Geochem. Geophys. Geosyst.* **19**, 21–42 (2018).
4. M. Amor, F. P. Mathon, C. L. Monteil, V. Busigny, C. T. Lefevre, Iron-biomineralizing organelle in magnetotactic bacteria: Function, synthesis and preservation in ancient rock samples. *Environ. Microbiol.*, 10.1111/1462-2920.15098 (2020).
5. M. Preiner *et al.*, A hydrogen-dependent geochemical analogue of primordial carbon and energy metabolism. *Nat. Ecol. Evol.* **4**, 534–542 (2020).
6. A. Roldan *et al.*, Bio-inspired CO₂ conversion by iron sulfide catalysts under sustainable conditions. *Chem. Commun. (Camb.)* **51**, 7501–7504 (2015).
7. B. E. Strauss, J. M. Feinberg, C. L. Johnson, Magnetic mineralogy of the Mercurian lithosphere. *J. Geophys. Res. Planets* **121**, 2225–2238 (2016).
8. R. Walker, A. D. Steele, D. T. B. Morgan, Deactivation of pyrophoric iron sulfides. *Ind. Eng. Chem. Res.* **36**, 3662–3667 (1997).
9. M. F. Hochella Jr *et al.*, Nanominerals, mineral nanoparticles, and Earth systems. *Science* **319**, 1631–1635 (2008).
10. A. Navrotsky, C. Ma, K. Lilova, N. Birkner, Nanophase transition metal oxides show large thermodynamically driven shifts in oxidation-reduction equilibria. *Science* **330**, 199–201 (2010).
11. K. Lilova, M. T. DeAngelis, L. M. Anovitz, A. Navrotsky, Surface energy of fayalite and its effect on Fe-Si-O oxygen buffers and the olivine-spinel transition. *Am. Mineral.* **103**, 1599–1603 (2018).
12. M. Y. Zolotov *et al.*, The redox state, FeO content, and origin of sulfur-rich magmas on Mercury. *J. Geophys. Res. Planets* **118**, 138–146 (2013).
13. S. Huang, D. Kang, X. Wu, J. Niu, S. Qin, Pressure-induced structural and spin transitions of Fe₃S₄. *Sci. Rep.* **7**, 46334 (2017).
14. R. A. Susilo *et al.*, Pressure-induced structural and electronic transitions of thiospinel Fe₃S₄. *J. Phys. Condens. Matter* **31**, 095401 (2019).
15. H. Xu, Z. Shen, H. Konishi, Natural occurrence of monoclinic Fe₃S₄ nano-precipitates in pyrrhotite from the Sudbury ore deposit: A Z-contrast imaging and density functional theory study. *Mineral. Mag.* **79**, 377–385 (2015).
16. F. Xu, A. Navrotsky, Enthalpies of formation of pyrrhotite Fe_{1–0.125x}S (0 ≤ x ≤ 1) solid solutions. *Am. Mineral.* **95**, 717–723 (2010).
17. A. H. Tavakoli, A. Navrotsky, Enthalpies of formation of Fe-Ni monosulfide solid solutions. *Am. Mineral.* **98**, 1508–1515 (2013).
18. M. Abramchuk, K. Lilova, T. Subramani, R. Yoo, A. Navrotsky, Development of high-temperature oxide melt solution calorimetry for p-block element containing materials. *J. Mater. Res.* **35**, 2239–2246 (2020).
19. S. Hayun, K. Lilova, S. Salhov, A. Navrotsky, Enthalpies of formation of high entropy and multicomponent alloys using oxide melt solution calorimetry. *Intermetallics* **125**, 1–7 (2020).
20. L. G. Benning, R. T. Wilkin, H. L. Barnes, Reaction pathways in the Fe–S system below 100°C. *Chem. Geol.* **167**, 25–51 (2000).
21. S.-J. Kao, C.-S. Horng, A. P. Roberts, K.-K. Liu, Carbon-sulfur-iron relationships in sedimentary rocks from southwestern Taiwan: Influence of geochemical environment on greigite and pyrrhotite formation. *Chem. Geol.* **203**, 153–168 (2004).
22. C. L. Blanchet, N. Thouveny, L. Vidal, Formation and preservation of greigite (Fe₃S₄) in sediments from the Santa Barbara basin: Implications for paleoenvironmental changes during the past 35 ka. *Paleoceanography* **24**, PA2224 (2009).
23. K. I. Lilova, C. I. Pearce, K. M. Rosso, A. Navrotsky, Energetics of spinels in the Fe-Ti-O system at the nanoscale. *ChemPhysChem* **15**, 3655–3662 (2014).
24. S. K. Sahu, B. Huang, K. Lilova, B. F. Woodfield, A. Navrotsky, Thermodynamics of Fe₃O₄-Co₃O₄ and Fe₃O₄-Mn₃O₄ spinel solid solutions at the bulk and nanoscale. *Phys. Chem. Chem. Phys.* **17**, 22286–22295 (2015).
25. A. Gorlas *et al.*, Greigite nanocrystals produced by hyperthermophilic archaea of Thermococcales order. *PLoS One* **13**, e0201549 (2018).
26. D. A. Kitchaev, G. Ceder, Evaluating structure selection in the hydrothermal growth of Fe₂S pyrite and marcasite. *Nat. Commun.* **7**, 13799 (2016).
27. C. Arrouvel, J. G. Eon, Understanding the surfaces and crystal growth of pyrite FeS₂. *Mater. Res.* **22**, 1–9 (2018).
28. K. Igarashi, Y. Yamamura, T. Kuwabara, Natural synthesis of bioactive greigite by solid-gas reactions. *Geochim. Cosmochim. Acta* **191**, 47–57 (2016).
29. L. R. Nittler *et al.*, The major-element composition of Mercury's surface from MESSENGER X-ray spectrometry. *Science* **333**, 1847–1850 (2011).
30. L. G. Evans *et al.*, Major-element abundances on the surface of Mercury: Results from the MESSENGER gamma-ray spectrometer. *J. Geophys. Res. Planets* **117**, E00L07 (2012).
31. A. R. Vasavada, D. A. Paige, S. E. Wood, Near-surface temperatures on Mercury and the Moon and the stability of polar ice deposits. *Icarus* **141**, 179–193 (1999).
32. L. Chang *et al.*, Low-temperature magnetic properties of greigite (Fe₃S₄). *Geochem., Geophys. Geosyst.* **10**, Q01Y04 (2009).
33. J. Schneider, H. de Wall, A. Kontny, T. Bechstädt, Magnetic susceptibility variations in carbonates of the La Vid Group (Cantabrian Zone, NW-Spain) related to burial diagenesis. *Sediment. Geol.* **166**, 73–88 (2004).
34. J. Cuda *et al.*, Low-temperature magnetic transition in troilite: A simple marker for highly stoichiometric FeS systems. *J. Geophys. Res. Solid Earth* **116**, B11205 (2011).
35. C. L. Johnson *et al.*, Planetary science. Low-altitude magnetic field measurements by MESSENGER reveal Mercury's ancient crustal field. *Science* **348**, 892–895 (2015).
36. D. L. Domingue *et al.*, Mercury's weather-beaten surface: Understanding Mercury in the context of Lunar and asteroidal space weathering studies. *Space Sci. Rev.* **181**, 121–214 (2014).
37. S. L. Murchie *et al.*, Orbital multispectral mapping of Mercury with the MESSENGER Mercury dual imaging system: Evidence for the origins of plains units and low-reflectance material. *Icarus* **254**, 287–305 (2015).
38. M. A. Valdez-Grijalva, L. Nagy, A. R. Muxworthy, W. Williams, K. Fabian, The magnetic structure and palaeomagnetic recording fidelity of sub-micron greigite (Fe₃S₄). *Earth Planet. Sci. Lett.* **483**, 76–89 (2018).
39. K. Righter, M. J. Drake, E. R. D. Scott, Compositional relationships between meteorites and terrestrial planets. *Meteorites Early Sol. Syst. II* **943**, 803–828 (2006).
40. D. S. McKay *et al.*, Search for past life on Mars: Possible relic biogenic activity in martian meteorite ALH84001. *Science* **273**, 924–930 (1996).
41. A. Ludwig, W. Zarek, E. Popiel, A. Winiarski, The study of meteorites by the X-ray, Mossbauer effect, XPS and magnetostatic methods. *Mol. Phys. Reports* **30**, 86–93 (2000).
42. G. Li *et al.*, High-purity Fe₃S₄ greigite microcrystals for magnetic and electrochemical performance. *Chem. Mater.* **26**, 5821–5829 (2014).
43. J. Liu *et al.*, Fe₃S₄ nanoparticles for arterial inflammation therapy: Integration of magnetic hyperthermia and photothermal treatment. *Appl. Mater. Today* **18**, 100457 (2020).
44. X. Zhang *et al.*, CuCo₂S₄ nanocrystals as a nanoplatform for photothermal therapy of arterial inflammation. *Nanoscale* **11**, 9733–9742 (2019).
45. B. Li *et al.*, Ultrasmall CuCo₂S₄ nanocrystals: All-in-one theragnosis nanoplatform with magnetic resonance/near-Infrared imaging for efficiently photothermal therapy of tumors. *Adv. Funct. Mater.* **27**, 1–10 (2017).
46. E. Stoyanov, U. Häussermann, K. Leinenweber, Large-volume multianvil cells designed for chemical synthesis at high pressures. *High Press. Res.* **30**, 175–189 (2010).
47. B. H. Toby, R. B. Von Dreele, GSAS-II: The genesis of a modern open-source all purpose crystallography software package. *J. Appl. Cryst.* **46**, 544–549 (2013).
48. K. Momma, F. Izumi, VESTA: A three-dimensional visualization system for electronic and structural analysis. *J. Appl. Cryst.* **41**, 653–658 (2008).
49. A. Navrotsky, Progress and new directions in calorimetry: A 2014 perspective. *J. Am. Ceram. Soc.* **97**, 3349–3359 (2014).
50. A. Navrotsky, Mineralogy, materials science, energy, and environment: A 2015 perspective. *Am. Mineral.* **100**, 674–680 (2015).
51. A. Navrotsky, Progress and new directions in high temperature calorimetry revisited. *Phys. Chem. Miner.* **24**, 222–241 (1997).